frontiers | Frontiers in Materials

ORIGINAL RESEARCH
published: 26 April 2022
doi: 10.3389/fmats.2022.864849

# Infrared Heating for Rapid and Localized Shape Transformations of Additively Manufactured Polymer Parts

*Seo-Hyeon Oh*[1], *Bona Goo*[1,2] *and Keun Park*[1]*

[1]Department of Mechanical System Design Engineering, Seoul National University of Science and Technology, Seoul, South Korea, [2]Energy Storage System Unit, SK Innovation Co. Ltd., Daejon, South Korea

Four-dimensional (4D) printing is an advanced application of additive manufacturing which enables additional shape transformations over time in response to external stimuli. For appropriate shape transformation, dedicated materials such as shape memory polymers or 3D printers supporting multi-material printing have been used. Recently, a facile 4D printing method was developed which used a fused filament fabrication type 3D printer and a plain thermoplastic filament. This method used the anisotropic thermal deformation of the FFF-printed part to intentionally impose anisotropy by programming orthogonal printing paths, which resulted in thermoresponsive shape transformation upon a thermal stimulation. While the previous studies used convective heating as the thermal stimulus and thus required a long heating time of more than 10 min, this study uses an infrared (IR) heating to enable rapid thermoresponsive shape transformation. An infrared heating system was developed which included an optical focusing unit, a masking unit and a movable heating stage. To investigate the speed of shape transformation, IR heating was performed on a rectangular strip (60 × 6 × 1.6 mm) and the relevant shape transformation time was compared with the previous convective heating result. The shape transformation proceeded rapidly, and after 70 s formed a fully-closed circular shape, corresponding to the 1/10 reduction compared with the convection type heating (more than 13 min). The IR heating was further applied to 2D-to-3D shape transformations of 2D star-shape and flower-shape specimens. For each specimen, a profiled mask was used to selectively irradiate IR on predefined regions and thus to localize the relevant thermoresponsive shape transformation. The global and local IR irradiations were then compared in terms of heating capability and the variability in shape transformations.

**Keywords: additive manufacturing, 4D printing, thermoresponsive shape transformation, fused filament fabrication, infrared heating**

OPEN ACCESS

***Edited by:***
*Stefano Pandini,*
*University of Brescia, Italy*

***Reviewed by:***
*Xiao Kuang,*
*Georgia Institute of Technology, United States*
*Irene Buj-Corral,*
*Universitat Politecnica de Catalunya, Spain*

***Correspondence:**
*Keun Park*
*kpark@seoultech.ac.kr*

***Specialty section:***
*This article was submitted to Smart Materials, a section of the journal Frontiers in Materials*

***Received:*** *28 January 2022*
***Accepted:*** *31 March 2022*
***Published:*** *26 April 2022*

***Citation:***
*Oh S-H, Goo B and Park K (2022) Infrared Heating for Rapid and Localized Shape Transformations of Additively Manufactured Polymer Parts. Front. Mater. 9:864849. doi: 10.3389/fmats.2022.864849*

## 1 INTRODUCTION

Four-dimensional (4D) printing is an advanced application of 3D printing, also known as additive manufacturing (AM), by transforming the shapes of additively manufactured parts over time (Tibbits. 2014; Mitchell et al., 2018; Demoly et al., 2021). The basic elements of 4D printing are external stimuli, stimulus-responsive materials, and interaction mechanisms (Momeni et al., 2017).

Various combinations of stimuli and stimulus-responsive materials have been studied to develop 4D printing for smart devices or functional actuators (Kuang et al., 2019).

The most popular stimuli in 4D printing are water and heat, and the relevant stimulus-responsive materials have been used to realize desired shape transformations (Ding et al., 2019). As a water-responsive material, hydrogel has been widely applied, utilizing its unique swelling characteristics in water (Bakarich et al., 2015; Dickey, 2016; Champeau et al., 2020). As a thermoresponsive material, shape memory polymer (SMP), which recovers its original shape by a thermal stimulus, has been used (Li and Huang, 2010; Kuang et al., 2018; Mehrpouya et al., 2021). Another method of thermoresponsive shape transformation is the AM of multi-materials that have different thermal expansion properties (Ding et al., 2018; Chen et al., 2019; Rafiee et al., 2020; Ren et al., 2021), which requires a 3D printer to support multi-material AM.

Recently, thermoresponsive 4D printing has also been developed based on single material AM and plain thermoplastic filaments without a shape memory function, by programming printing paths in a material extrusion (ME) type AM process. The ME type AM process, also known as fused filament fabrication (FFF) or fused deposition modeling (FDM), is based on the extrusion of a thermoplastic filament through a thin nozzle. The resulting extruded strands undergo residual stress: tensile residual stress along the printing direction and compressive residual stress along the lateral direction. The printing paths have been programmed to induce anisotropy along unidirectional (Bodaghi et al., 2017; Hu et al., 2017; Rajkumar and Shanmugam, 2018; Bodaghi et al., 2019; Goo et al., 2021) or bidirectional (Van Manen et al., 2017; Goo et al., 2020) laminations. Accordingly, a part printed via a specially programmed printing path deforms when an appropriate thermal stimulus is applied to release the residual stress, which results in one-way irreversible shape transformation unlike the conventional 4D printing methods that use smart materials.

As a thermal stimulus, convective heating has generally been used by immersing an anisotropically printed sample in hot water (Bodaghi et al., 2017; Hu et al., 2017; Bodaghi et al., 2019). For an acrylonitrile butadiene styrene (ABS) sample, on the other hand, an electric oven was used for the convective heating (Goo et al., 2020; Goo et al., 2021) because its glass transition temperature is higher than 100 °C. Although these convective heating methods provide uniform heating capability, their thermal responses are relatively slow due to the low convection coefficient of air. For example, the previous study (Rajkumar and Shanmugam, 2018; Goo et al., 2020) required more than 10 min heating to accomplish the thermoresponsive shape transformations of bilayer ABS samples.

To increase the speed of the thermoresponsive shape transformation of anisotropically printed FFF parts, this study used IR heating as a thermal stimulus instead of the conventional convective heating. IR heating has been used to heat polymer materials for various polymer processing methods, including injection molding (Saito et al., 2002), stretch-blow molding (Bordival et al., 2009), and thermoforming (Lee et al., 2017). It has also been used in the FFF type AM process to improve the interlayer strength and mechanical strength of polymer parts (Kishore et al., 2017; Ravoori et al., 2019; Nycz et al., 2020; Lee et al., 2021).

**TABLE 1 |** Anisotropic material properties of additively manufactured ABS specimens.

| Direction | $E$ (GPa) | $\sigma_u$ (MPa) | $\alpha_l$ ($\times10^{-3}$/°C) | $\alpha_t$ ($\times10^{-3}$/°C) |
|---|---|---|---|---|
| Length ($x$) | 2.178 | 28.47 | -1.53 | 0.16 |
| Width ($y$) | 2.497 | 33.47 | 0.95 | -0.40 |
| Height ($z$) | 2.258 | 8.39 | 2.22 | 2.22 |

In this study, IR heating was used to heat additively manufactured bilayer specimens for rapid shape transformation. The IR heating was further applied for localized heating and shape transformation using an auxiliary profile mask, which can distinguishes this approach from existing 4D printing studies involving local heating capability. Three bilayer specimens (a rectangular bar, a star-shape plate, and a flower shape plate) were additively manufactured by programming printing paths to have the intended orthogonal anisotropy. The IR heating was then applied via global and local irradiations, and the relevant deformation characteristics of the three specimens were investigated. Experimental analyses showed that the proposed method has unique characteristics including rapid, localized, and irreversible shape transformations, which are advantageous for practical 4D printing. The use of plain thermoplastic material (ABS) and a personal FFF type 3D printer is also useful to accelerate the practical use of 4D printing.

# 2 MATERIALS AND METHODS

## 2.1 Materials

A white ABS filament of 1.75 mm diameter (Shenzhen ESUN Industrial Co. Ltd., China) was used in the FFF type AM. Its density, melting temperature and glass transition temperature were 1.04 g/cm$^3$, 230 and 107.8°C, respectively. Additively manufactured parts using this filament are known to have orthotropic anisotropy in mechanical properties including elastic modulus ($E$) and tensile strength ($\sigma_u$), as listed in **Table 1** (Lim et al., 2017). It has been also reported that the AM of this filament resulted in anisotropy in the apparent thermal expansion coefficients when the printing path was programmed to be unidirectional, either along the longitudinal or transverse directions (Goo et al., 2020). The relevant thermal expansion coefficients along the longitudinal ($\alpha_l$) and transverse ($\alpha_t$) directions are given in **Table 1** (Goo et al., 2021). To enhance light absorption in IR heating, a black ABS filament (Shenzhen ESUN Industrial Co. Ltd., China) was also used and the resulting heating capability was compared to that of the white one.

## 2.2 Additive Manufacturing With Programmed Printing Path

An FFF type 3D printer (Cubicon Single, Cubicon Inc., Korea) was used to fabricate preliminary specimens for 4D printing. This printer uses an extrusion nozzle with a diameter of 0.4 mm through

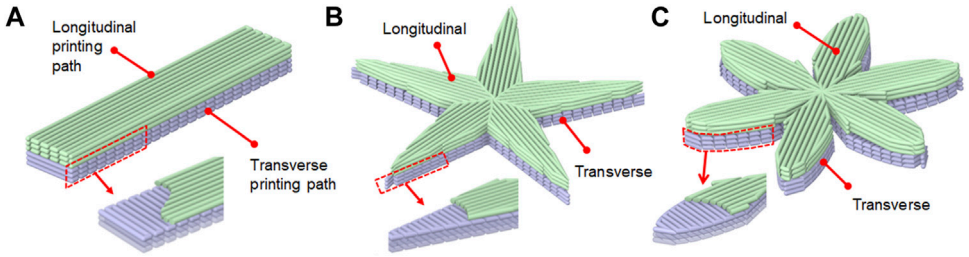


**FIGURE 1 |** Programmed printing paths of bilayer specimens **(A)** Rectangular bar **(B)** Star-shape plate **(C)** Flower-shape plate.

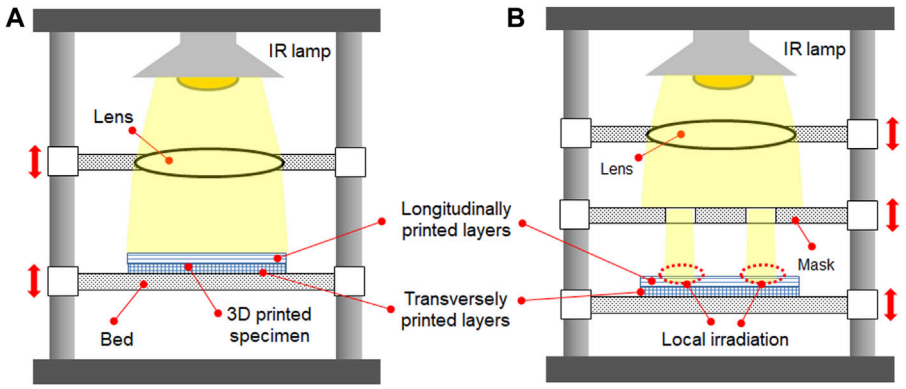


**FIGURE 2 |** Configuration of the IR heating system for thermoresponsive shape transformation **(A)** Global IR irradiation **(B)** Local IR irradiation using a profiled mask.

which a filament with 1.75 mm diameter is extruded. In FFF-type AM, the layer thickness and printing speed were set to 0.2 and 80 mm/s, respectively. The hatch distance was set to 0.4 mm, which corresponded to 100% infill density. For stable printing with ABS filaments, the temperatures of the extrusion nozzle, printing bed and printer chamber were set to 240, 110, and 60°C, respectively.

Three preliminary specimens were printed to induce thermosresponsive shape transformations, as demonstrated in **Figure 1A–C**. In each specimen, the printing path was programmed to construct a bilayer structure, which included a number of layers printed along the transverse (i.e., 90° raster angle) and longitudinal (i.e., 0° raster angle) printing paths. **Figure 1A** shows the bilayer printing paths for a rectangular bar (60 × 6 × 1.6 mm), which includes four transversely printed layers and four longitudinally printed layers. This specimen was designed to observe 1D-to-2D shape transformation, and to compare the transformation speed with that of the previous 4D printing method under convective heating (Goo et al., 2020). **Figure 1B,C** show the printing paths for the 2D star and flower shapes, respectively. Here, the printing regions were divided by considering their rotationally repeated structures. For each printing region, the printing paths were programmed to have three transverse layers and three longitudinal layers, and thus 2D-to-3D thermoresponsive shape transformations are expected.

## 2.3 Infrared Heating

An infrared (IR) heating system was developed to heat the additively manufactured bilayer specimens. **Figure 2A** shows the IR heating system that consists of an IR lamp, a convex lens, and a printing bed. The lens and bed were designed to be vertically movable with the aid of linear actuators, and thus the size of the heating region can be adjusted according to the size of the specimen. **Figure 2B** shows the IR heating system used for local irradiation, wherein a mask plate was additionally installed between the lens and bed. The mask plate was designed to have holes or slots through which IR rays could selectively irradiate the specimen.

Two types of IR lamps were used depending on the specimen shape. For the rectangular bar specimen, a line lamp (500 W) was used to effectively heat the bar specimen. For the 2D plate specimens (i.e., the star and flower specimens), a point lamp (100 W) was used with a concave reflector. Here, the vertical positions of the lens and bed were controlled to adjust the diameter of the irradiation to cover the specimen size. A thermal imaging system (FLIR E50, FLIR Systems Inc., United States) was used to measure temperature changes in the bilayer specimens during the IR heating process.

# 3 RESULTS

## 3.1 1D-to-2D Shape Transformations of a Rectangular bar

The rectangular bar specimen in **Figure 1A** was heated using the IR heating system in **Figure 2**. Both the global and local IR

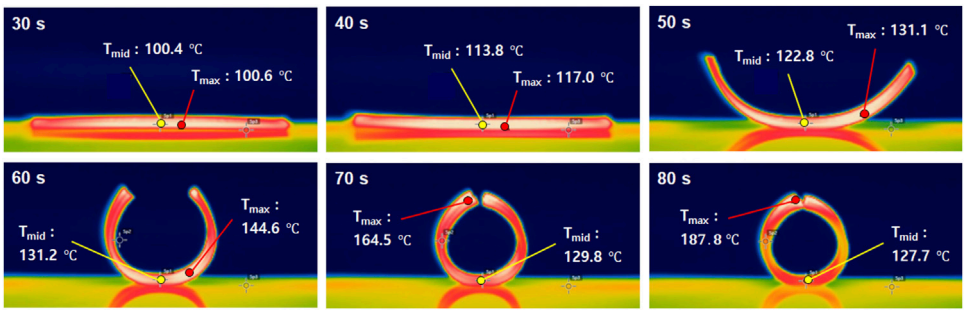


**FIGURE 3 |** Global shape transformations of a bilayer bar with increasing IR irradiation time. Here, $T_{mid}$ and $T_{max}$ indicate the temperatures at the midpoint and at the maximum temperature point, respectively.

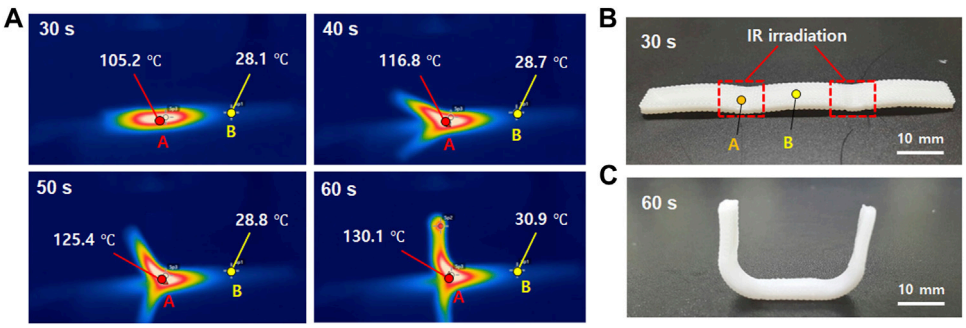


**FIGURE 4 |** Local shape transformations of a bilayer bar **(A)** Temperature change with increasing IR irradiation time **(B)** Deformed shape after 30 s heating **(C)** Deformed shape after 60 s heating. Here, points A and B indicate the unmasked and masked locations for IR irradiation, respectively.

irradiations were conducted as demonstrated in **Figure 2A,B**. For the local IR irradiation, a profiled mask was prepared with two rectangular holes of 10 × 10 mm. The relevant 1D-to-2D shape transformation results are discussed in the following subsections.

### 3.1.1 Global Shape Transformation

**Figure 3** shows IR camera images with increasing IR irradiation time. Here, $T_{mid}$ and $T_{max}$ indicate the temperatures at the midpoint and the maximum temperature point, respectively. It can be seen that the left end of the bar begins to bend after 40 s heating, which indicates that the specimen was heated enough to initiate thermal deformation, overcoming its own weight. It is notable that both the temperatures ($T_{mid}$ and $T_{max}$) at 40 s heating were higher than the glass transition temperature of the ABS, 107.8°C.

This bending deformation occurred due to the difference in thermal deformation of the upper and lower regions of the specimen. That is, the transversely printed lower layers were lengthened while the longitudinally printed upper layers were shortened due to their intrinsic residual stresses. This bending deformation continued as irradiation time increased, and after 70 s the specimen was rolled into a circular shape, as shown in **Figure 3**. The proposed IR heating achieved ten times faster heating speed than the previous convective heating, which required 13 min heating time (Goo et al., 2020).

### 3.1.2 Local Shape Transformation

**Figure 4A** shows IR camera images of the left side of the bar, with increasing IR irradiation time. Here, point A is the midpoint of the irradiated region and point B is in the masked region where IR rays do not reach, as shown in **Figure 4B**. The distance between points A and B was set to 15 mm. It can be seen that the temperature of point A reached 105.2°C while that of point B was as low as 28.1 °C at 30 s heating.

The left end of the bar began to bend after 40 s heating, and the corresponding temperature at point A was 116.8°C, a value higher than the glass transition temperature (107.8°C). This localized bending continued with an increase in irradiation time, and the specimen was bent vertically after 60 s heating. The corresponding temperature difference between the points A and B was 99.2°C, which indicates that the IR heating can be localized on the selectively irradiated regions. The localized heating then induces a localized shape transformation, as shown in **Figure 4C**. Compared to the results with global IR heating (**Figure 3**), the use of a profiled mask enables localized heating and bending deformation, which further increases the diversity of the shape transformations of the proposed 4D printing method.

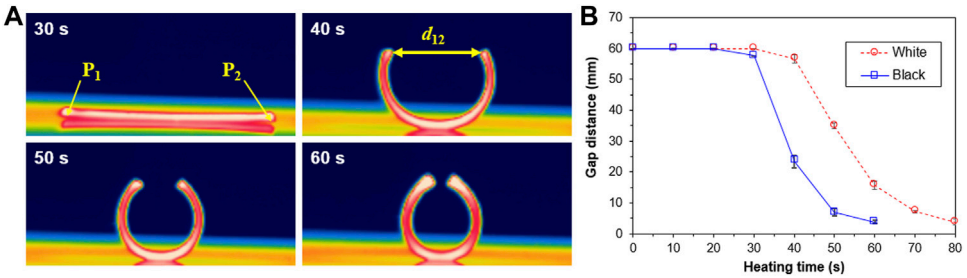


**FIGURE 5 |** Global shape transformation of the black rectangular bar specimen **(A)** Deformations and the relevant temperature changes **(B)** Comparison of the gap distances of the black and white specimens.

### 3.1.3 Shape Transformations of Differently Coloured Specimens

To investigate the effect of light absorption characteristics on heating capability, IR heating was also conducted on rectangular bar specimens printed with black filaments. The printing and IR heating conditions were set to be the same as the previous case that used white filaments. **Figure 5A** shows stepwise IR camera images, which reveal that the transformation speed was higher than with the white filament, in **Figure 3**. To compare the transformation speed quantitatively, the gap distance between points $P_1$ and $P_2$ ($d_{12}$ in **Figure 5A**) was measured as heating time increased. The heating experiments were conducted with five specimens to confirm the repeatability of the shape transformation.

**Figure 5B** compares the changes in gap distance ($d_{12}$) of the black and white specimens. The gap distance of the black specimen declines significantly faster than that of the white specimen. The resulting gap distance of the black specimen was 3.81 ± 0.55 mm at 60 s heating, and exhibited an almost closed shape. In contrast, the white specimen exhibited a gap distance of 15.84 ± 1.41 mm at 60 s heating, and was transformed into a closed shape after 70 s heating, with a gap distance of 7.22 ± 0.40 mm. This result indicates that the black filament is more efficient for IR heating than the white filament, because of its superior light absorption capability (Manara et al., 2011). Based on these results, the following 2D-to-3D shape transformations were conducted using the black filament, since they required large volumes to be heated.

## 3.2 2D-to-3D Shape Transformations

The proposed IR-based 4D printing method was then applied to 2D-to-3D shape transformations, for the 2D star and flower shapes in **Figures 1B,C**. The relevant global and local shape transformation results of each specimen are discussed in the following subsections.

### 3.2.1 Shape Transformations of a Star-Shape Plate

**Figure 6A** shows a photograph of the additively manufactured 2D star-shape plate. Here, the marked region is magnified for the lower and upper layers, which were printed along the transverse and longitudinal paths, respectively. **Figure 6B** shows the mask design for local heating of the star-shape specimen. The mask has a circular shape with an outer diameter of 90 mm, and has five annular slots inside. Accordingly, IR rays reach the specimen through these slots, and the IR heating is focused on the selected regions. **Figure 6C** shows the deformed shape of the star-shape plate, after 300 s heating under global IR irradiation. It can be seen that the five arms are bent upward to form a smooth curvature. With local heating, on the other hand, the bending effects are localized in the five irradiated regions, and the relevant shape forms sharp bends, as shown in **Figure 6D**.

**Figure 7A** shows IR camera images of the 2D star-shape plate during the global shape transformation. It can be seen that the five arms lift after 120 s heating, when the body temperature increases higher than 110°C. The initiation of the bending deformation is much slower than that of the rectangular bar in **Figure 3** because the power of the point-type IR lamp (100 W) is lower than that of the line-type IR lamp (500 W). **Figure 7B** compares the temperature profiles of the points C and D. It can be seen that the point D has a higher temperature than point C until 120 s of heating, because the light intensity in the centre region (point D) is higher than in the surrounding region. This trend is reversed after 120 s heating, at which point the shape transformation initiates and the arm parts are lifted. Accordingly, point C moves closer to the light source than point B, and thus shows a higher heating rate. After 240 s heating, the maximum temperatures of points C and D are 152.2 and 147.3°C, respectively.

**Figure 8A** shows IR camera images of the 2D star-shape plate during the local shape transformation. It can be seen that the five irradiated regions are locally heated, and the resulting bending deformation proceeds only in the locally heated regions. **Figure 8B** compares the temperature profiles of points C and D, which shows that the heating rate of the irradiated region (point C) is remarkably faster than that of the masked region (point D). The temperatures of points C and D after 240 s heating are 123.6 and 86.7°C, respectively. The temperature difference between these two points is 36.9°C, which is much higher than that of the global IR heating, 4.9°C. Accordingly, the local IR irradiation can selectively heat desired regions, and thus can effectively control the resulting shape transformation.

### 3.2.2 Shape Transformations of a Flower Shape Plate

**Figure 9A** shows a photograph of the additively manufactured 2D flower-shape plate. Magnified photographs of the lower and upper layers are also provided to verify the relevant printing

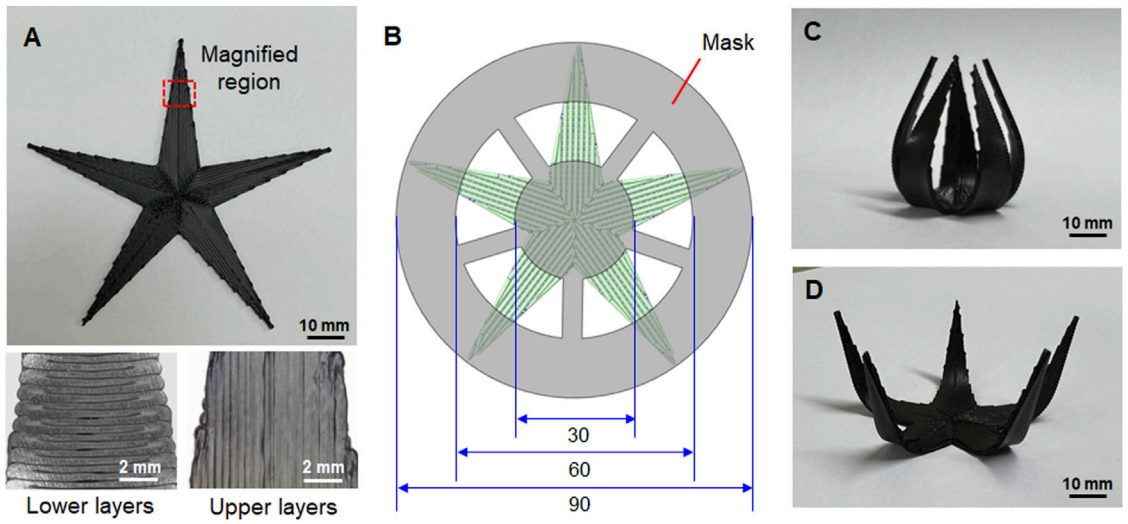


**FIGURE 6 |** Shape transformations of the 2D star-shape plate **(A)** Additively manufactured star-shape specimen **(B)** Mask design for local irradiation (unit: mm) **(C)** Deformed shape after global IR irradiation **(D)** Deformed shape after local IR irradiation. Here, IR irradiation time was set to 300 s for each case.

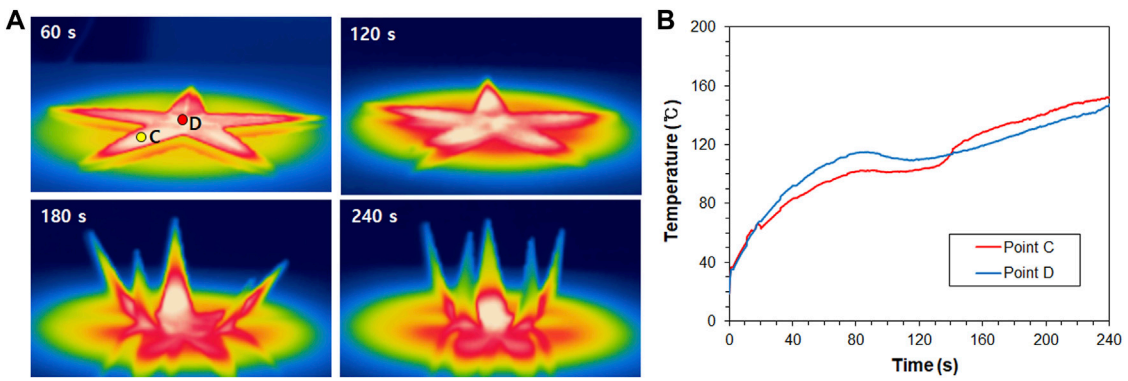


**FIGURE 7 |** Global shape transformation of the 2D star-shape plate **(A)** Deformations and the relevant temperature changes **(B)** Comparison of temperature profiles at points C and D.

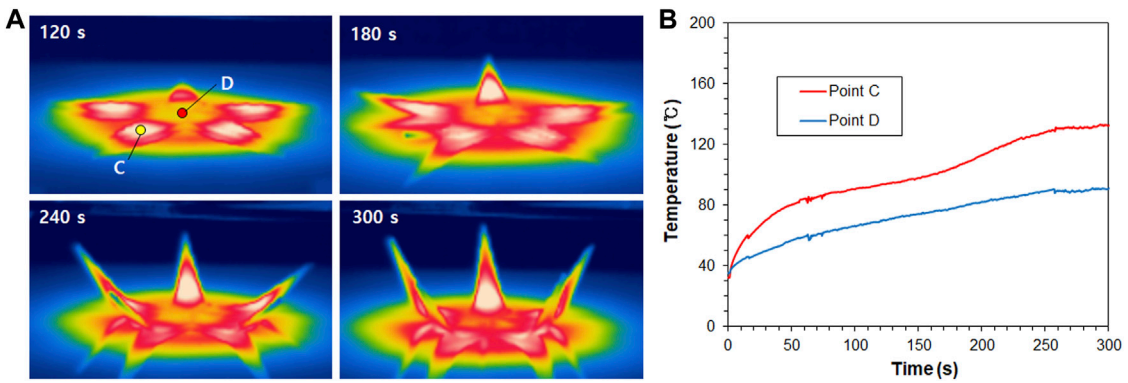


**FIGURE 8 |** Local shape transformation of the 2D star-shape plate **(A)** Deformations and the relevant temperature changes **(B)** Comparison of temperature profiles at points C and D.

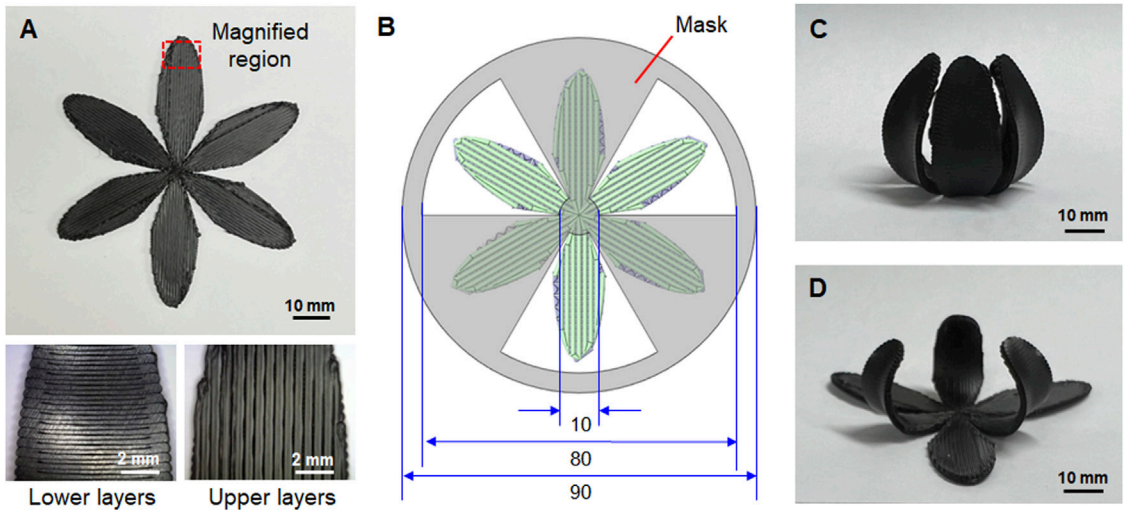


**FIGURE 9 |** Shape transformations of the 2D flower-shape plate **(A)** Additively manufactured flower-shape specimen **(B)** Mask design for the local irradiation (unit: mm) **(C)** Deformed shape after global IR irradiation **(D)** Deformed shape after local IR irradiation. Here, IR irradiation time was set to 300 s for each case.

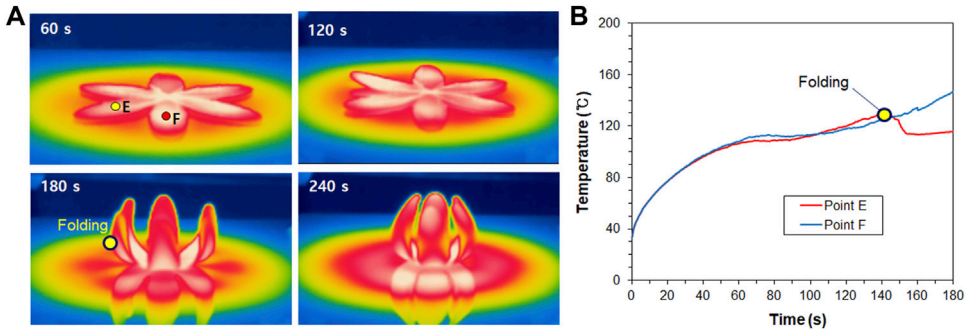


**FIGURE 10 |** Global shape transformation of the 2D flower-shape plate **(A)** Deformations and the relevant temperature changes **(B)** Comparison of temperature profiles at points E and F.

paths. **Figure 9B** shows the mask design for local heating of the flower-shape specimen. The mask has a circular shape with an outer diameter of 90 mm, and has three annular slots to cover three petals. Accordingly, IR rays reach the specimen through these three slots, and the IR heating is focused on the corresponding three petals. **Figure 9C** shows the deformed shape after 300 s heating under global IR irradiation. It can be seen that all six petals are bent upward, mimicking petals being curled up. On the other hand, the bending deformation occurred only on the three selected petals with the local heating, as shown in **Figure 9D**.

**Figure 10A** shows IR camera images of the 2D flower-shape plate during the global shape transformation. As the heating time increases, the six petals bend upward and curl inside, mimicking a blooming motion in reverse. Two reference points on different petals, marked as points E and F in **Figure 10A**, were selected for temperature measurement. **Figure 10B** shows the temperature profiles at these reference points. Here, the maximum time was set to 180 s because all petals become folded and thus further temperature measurement would be inaccurate. While the two reference points had almost the same temperature profiles, point E showed a sudden temperature drop at around 140 s heating time. This abrupt temperature drop is due to the folding in the corresponding petal. On the other hand, the temperature at points E showed a steady increase to 124.5°C because the corresponding petal was not folded.

**Figure 11A** shows IR camera images of the 2D flower-shape plate during the local shape transformation. Here, point E is located in the IR irradiated region while point F is located in the masked region. It can be seen that the three petals in the irradiated regions are selectively heated, and undergo thermoresponsive shape transformations without folding until 300 s of heating. **Figure 11B** compares the temperature profiles of points E and F, which reveals that the irradiated region (point E) is heated faster than the masked region (point F). At 180 s heating time, the temperatures of points E and F are 116.3 and 65.4°C, respectively. The resulting temperature difference between these

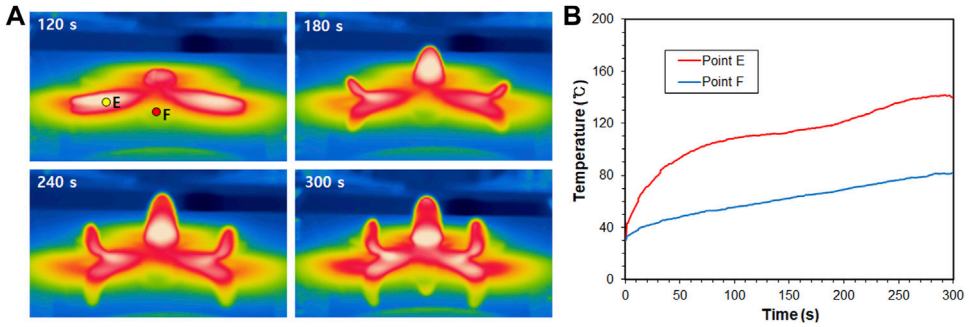


**FIGURE 11 |** Local shape transformation of the 2D flower-shape plate **(A)** Deformations and the relevant temperature changes **(B)** Comparison of temperature profiles at points E and F.

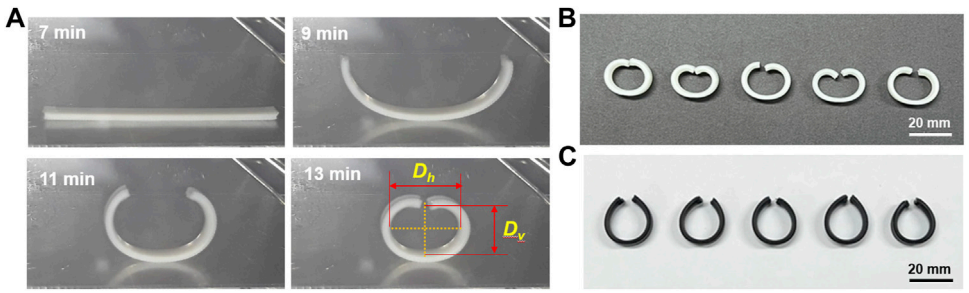


**FIGURE 12 |** Comparison with the convective heating results **(A)** Stepwise shape transformation of the rectangular bar (Goo et al., 2020) **(B)** Transformed specimens after 13 min convective heating (white ABS) **(C)** Transformed specimens after 60 s IR heating (black ABS).

two points is 50.9°C, which is much larger than that between the points C and D in **Figure 8**, 36.9°C. This occurs because the irradiated (point E) and masked (point F) regions are located in different petals, and the resulting heat transfer path is much longer than that of the previous star-shape specimen (i.e., between points C and D in **Figure 8A**).

## 4 DISCUSSION

To discuss the transformation speed of the proposed IR-based 4D printing, the shape shifting kinetics of the rectangular bar specimen were compared with those of the previous 4D printing using convective heating. **Figure 12A** shows the stepwise shape transformations with convective heating (Goo et al., 2020); the printing material and conditions were the same as in this study. As discussed in **Section 3.1.1**, the convective heating required more than 13 min (i.e., 780 s) to form a closed shape, which was ten times longer than the proposed IR heating (70 s). This long transformation time was also reported in a previous study (Rajkumar and Shanmugam, 2018), which required 15 min to induce shape transformation in a 50 mm bar specimen.

Besides the low transformation speed, the convective heating resulted in deformation into an elliptical shape, where the horizontal diameter ($D_h$) was larger than the vertical diameter ($D_v$). The apparent roundness was defined by the ratio of the vertical to the horizontal diameters ($D_v/D_h$). **Figure 12B** shows photographs of five transformed specimens after 780 s convective heating (white ABS). The horizontal and vertical diameters were measured to be 16.65 ± 1.81 and 10.31 ± 1.35 mm, respectively, and the resulting roundness was calculated to be 62.4 ± 9.85%. Since pure bending generally transforms into a circular shape (Zou et al., 2021), this elliptic shape transformation depends on more complicate deformation mechanism, related to the low heating speed and forced air flow during convective heating (Rajkumar and Shanmugam, 2018; Goo et al., 2020).

**Figure 12C** shows five transformed specimens after 60 s IR heating (black ABS), in which all specimens were transformed to nearly circular shapes. The horizontal and vertical diameters were measured to be 15.40 ± 0.28 mm and 16.76 ± 0.19 mm, respectively, and the resulting roundness value increased to 108.8 ± 2.58%. This indicates that the IR heating resulted in thermal deformation into a circular shape, which is close to the pure bending deformation. Furthermore, the IR heating showed less deviation in the transformed shape values (i.e., the horizontal and vertical diameters), which ensures better dimensional stability and repeatability than the convective heating.

## 5 CONCLUSION

In this study, a rapid 4D printing method was proposed based on FFF-type AM with IR heating. In the FFF-type AM process, the

printing path was programmed to have an orthogonal anisotropy by consecutively laminating a number of transversely and longitudinally printed layers, in 1D- or 2D-bilayer structures; a rectangular bar, a star-shape plate, and a flower-shape plate. These bilayer structures have unique thermal deformation characteristics, in which the transversely printed lower layers elongate while the longitudinally printed upper layers shrink. Under IR irradiation, the bilayer rectangular bar specimen was transformed into a circular shape. This shape transformation occurred in only 70 s, which corresponds to a ten-time faster speed than the previous method using convective heating (more than 13 min). Moreover, the change in the temperature distribution can be observed in real time, which was impossible in the convective heating in a closed chamber.

Another advantage of the IR-based 4D printing is that a target region can be selected by designing a mask profile accordingly, and thus the IR rays can be irradiated locally on selected areas. This local IR irradiation enables localized heating and resulting bending deformation, which also cannot be realized with convective heating. In addition to the aforementioned six transformation cases with three AM specimens and two IR irradiation methods (i.e., the global and local irradiations), various combinations of the printing paths and the mask designs can be further applied for versatile shape transformations.

Considering that long heating time and limited shape transformation are the disadvantages of the existing FFF-based 4D printing methods, the IR-based shape transformation with high heating speed, localized heating capability and irreversible thermal deformation is expected to expand the application areas of 4D printing technology in the future, including AM with curved geometries without support structures or to realize self-assembly structures. Further studies are required to investigate the various combinations of specimen shapes, printing paths and mask designs, and to broaden the deformation modes of shape transformations based on the various design requirements.

## DATA AVAILABILITY STATEMENT

The original contributions presented in the study are included in the article/Supplementary Materials, further inquiries can be directed to the corresponding author.

## AUTHOR CONTRIBUTIONS

KP conceived the idea and designed the research. SH-O and BG co-analyzed the experimental and calculated data. SH-O and KP contributed to the writing and editing of the manuscript. All authors contributed to the article and approved the submitted version content of the work.

## FUNDING

This study was financially supported by the National Research Foundation of Korea (NRF) grant funded by the Ministry of Science and ICT, Republic of Korea (Grant number: 2019R1A2C1002799).

## REFERENCES

Bakarich, S. E., Gorkin, R., III, Panhuis, M. i. h., and Spinks, G. M. (2015). 4D Printing with Mechanically Robust, Thermally Actuating Hydrogels. *Macromol. Rapid Commun.* 36, 1211–1217. doi:10.1002/marc.201500079

Bodaghi, M., Damanpack, A. R., and Liao, W. H. (2017). Adaptive Metamaterials by Functionally Graded 4D Printing. *Mater. Des.* 135, 26–36. doi:10.1016/j.matdes.2017.08.069

Bodaghi, M., Noroozi, R., Zolfagharian, A., Fotouhi, M., and Norouzi, S. (2019). 4D Printing Self-Morphing Structures. *Materials* 12, 1353. doi:10.3390/ma12081353

Bordival, M., Schmidt, F. M., Maoult, Y. L., and Velay, V. (2009). Optimization of Preform Temperature Distribution for the Stretch-Blow Molding of PET Bottles: Infrared Heating and Blowing Modeling. *Polym. Eng. Sci.* 49, 783–793. doi:10.1002/pen.21296

Champeau, M., Heinze, D. A., Viana, T. N., de Souza, E. R., Chinellato, A. C., and Titotto, S. (2020). 4D Printing of Hydrogels: a Review. *Adv. Funct. Mater.* 30, 1910606. doi:10.1002/adfm.201910606

Chen, X., Liu, X., Ouyang, M., Chen, J., Taiwo, O., Xia, Y., et al. (2019). Multi-metal 4D Printing with a Desktop Electrochemical 3D Printer. *Sci. Rep.* 9, 3973–3979. doi:10.1038/s41598-019-40774-5

Demoly, F., Dunn, M. L., Wood, K. L., Qi, H. J., and André, J.-C. (2021). The Status, Barriers, Challenges, and Future in Design for 4D Printing. *Mater. Des.* 212, 110193. doi:10.1016/j.matdes.2021.110193

Dickey, M. D. (2016). Shaped after Print. *Nat. Mater* 15, 379–380. doi:10.1038/nmat4608

Ding, Z., Weeger, O., Qi, H. J., and Dunn, M. L. (2018). 4D Rods: 3D Structures via Programmable 1D Composite Rods. *Mater. Des.* 137, 256–265. doi:10.1016/j.matdes.2017.10.004

Ding, H., Zhang, X., Liu, Y., and Ramakrishna, S. (2019). Review of Mechanisms and Deformation Behaviors in 4D Printing. *Int. J. Adv. Manuf. Technol.* 105, 4633–4649. doi:10.1007/s00170-019-03871-3

Goo, B., Hong, C.-H., and Park, K. (2020). 4D Printing Using Anisotropic thermal Deformation of 3D-Printed Thermoplastic Parts. *Mater. Des.* 188, 108485. doi:10.1016/j.matdes.2020.108485

Goo, B., Kim, J.-B., Ahn, D.-G., and Park, K. (2021). Irreversible and Repeatable Shape Transformation of Additively Manufactured Annular Composite Structures. *Materials* 14, 1383. doi:10.3390/ma14061383

Hu, G. F., Damanpack, A. R., Bodaghi, M., and Liao, W. H. (2017). Increasing Dimension of Structures by 4D Printing Shape Memory Polymers via Fused Deposition Modeling. *Smart Mater. Struct.* 26, 125023. doi:10.1088/1361-665x/aa95ec

Kishore, V., Ajinjeru, C., Nycz, A., Post, B., Lindahl, J., Kunc, V., et al. (2017). Infrared Preheating to Improve Interlayer Strength of Big Area Additive Manufacturing (BAAM) Components. *Additive Manufacturing* 14, 7–12. doi:10.1016/j.addma.2016.11.008

Kuang, X., Chen, K., Dunn, C. K., Wu, J., Li, V. C. F., and Qi, H. J. (2018). 3D Printing of Highly Stretchable, Shape-Memory, and Self-Healing Elastomer toward Novel 4D Printing. *ACS Appl. Mater. Inter.* 10, 7381–7388. doi:10.1021/acsami.7b18265

Kuang, X., Roach, D. J., Wu, J., Hamel, C. M., Ding, Z., Wang, T., et al. (2019). Advances in 4D Printing: Materials and Applications. *Adv. Funct. Mater.* 29, 1805290. doi:10.1002/adfm.201805290

Lee, H.-J., Shin, D.-J., and Park, K. (2017). Ultrasonic Thermoforming of a Large Thermoplastic Polyurethane Film with the Aid of Infrared Heating. *J. Mech. Sci. Technol.* 31, 5687–5693. doi:10.1007/s12206-017-1109-x

Lee, J. E., Park, S. J., Son, Y., Park, K., and Park, S.-H. (2021). Mechanical Reinforcement of Additive-Manufactured Constructs Using *In Situ*

Auxiliary Heating Process. *Additive Manufacturing* 43, 101995. doi:10.1016/j.addma.2021.101995

Li, S., and Huang, W. M. (2010). Mechanisms of the Multi-Shape Memory Effect and Temperature Memory Effect in Shape Memory Polymers. *Soft. Matter.* 6, 4403–4406.

Lim, Y.-E., Kim, N.-H., Choi, H.-J., and Park, K. (2017). Design for Additive Manufacturing of Customized Cast with Porous Shell Structures. *J. Mech. Sci. Technol.* 31, 5477–5483. doi:10.1007/s12206-017-1042-z

Manara, J., Reidinger, M., Rydzek, M., and Arduini-Schuster, M. (2011). Polymer-based Pigmented Coatings on Flexible Substrates with Spectrally Selective Characteristics to Improve the thermal Properties. *Prog. Org. Coat.* 70, 199–204. doi:10.1016/j.porgcoat.2010.09.024

Mehrpouya, M., Vahabi, H., Janbaz, S., Darafsheh, A., Mazur, T. R., and Ramakrishna, S. (2021). 4D Printing of Shape Memory Polylactic Acid (PLA). *Polymer* 230, 124080. doi:10.1016/j.polymer.2021.124080

Mitchell, A., Lafont, U., Hołyńska, M., and Semprimoschnig, C. (2018). Additive Manufacturing - A Review of 4D Printing and Future Applications. *Additive Manufacturing* 24, 606–626. doi:10.1016/j.addma.2018.10.038

Momeni, F., M.Mehdi Hassani.N, S., Liu, X., and Ni, J. (2017). A Review of 4D Printing. *Mater. Des.* 122, 42–79. doi:10.1016/j.matdes.2017.02.068

Nycz, A., Kishore, V., Lindahl, J., Duty, C., Carnal, C., and Kunc, V. (2020). Controlling Substrate Temperature with Infrared Heating to Improve Mechanical Properties of Large-Scale Printed Parts. *Additive Manufacturing* 33, 101068. doi:10.1016/j.addma.2020.101068

Rafiee, M., Farahani, R. D., and Therriault, D. (2020). Multi-Material 3D and 4D Printing: A Survey. *Adv. Sci.* 7, 1902307. doi:10.1002/advs.201902307

Rajkumar, A. R., and Shanmugam, K. (2018). Additive Manufacturing-Enabled Shape Transformations via FFF 4D Printing. *J. Mater. Res.* 33, 4362–4376. doi:10.1557/jmr.2018.397

Ravoori, D., Prajapati, H., Talluru, V., Adnan, A., and Jain, A. (2019). Nozzle-integrated Pre-deposition and post-deposition Heating of Previously Deposited Layers in Polymer Extrusion Based Additive Manufacturing. *Additive Manufacturing* 28, 719–726. doi:10.1016/j.addma.2019.06.006

Ren, L., Li, B., Liu, Q., Ren, L., Song, Z., Zhou, X., et al. (2021). 4D Printing Dual Stimuli-Responsive Bilayer Structure toward Multiple Shape-Shifting. *Front. Mater.* 8, 134. doi:10.3389/fmats.2021.655160

Saito, T., Satoh, I., and Kurosaki, Y. (2002). A New Concept of Active Temperature Control for an Injection Molding Process Using Infrared Radiation Heating. *Polym. Eng. Sci.* 42, 2418–2429. doi:10.1002/pen.11128

Tibbits, S. (2014). 4D Printing: Multi-Material Shape Change. *Archit Des.* 84, 116–121. doi:10.1002/ad.1710

Van Manen, T., Janbaz, S., and Zadpoor, A. A. (2017). Programming 2D/3D Shape-Shifting with Hobbyist 3D Printers. *Mater. Horiz.* 4, 1064–1069. doi:10.1039/c7mh00269f

Zou, Y., Huang, Z., Li, X., and Lv, P. (2021). 4D Printing Pre-strained Structures for Fast thermal Actuation. *Front. Mater.* 8, 661999. doi:10.3389/fmats.2021.661999

**Conflict of Interest:** Author BG is employed by SK Innovation Co. Ltd.

The remaining authors declare that the research was conducted in the absence of any commercial or financial relationships that could be construed as a potential conflict of interest.

**Publisher's Note:** All claims expressed in this article are solely those of the authors and do not necessarily represent those of their affiliated organizations, or those of the publisher, the editors and the reviewers. Any product that may be evaluated in this article, or claim that may be made by its manufacturer, is not guaranteed or endorsed by the publisher.